Influence of measuring geometry on rheomalaxis of macro-crystalline wax-oil gels: Alteration of breakage mechanism from adhesive to cohesive

Sandra Rodriguez-Fabia, Regina Lopez Fyllingsnes, Nicolai Winter-Hjelm, Jens Norrman, and Kristofer Gunnar Paso*

Ugelstad Laboratory, Department of Chemical Engineering, Norwegian University of Science and Technology (NTNU), Trondheim, Norway

E-mail: kristofer.g.paso@ntnu.no

Abstract

Rheological measurement of wax-oil gel breakage is highly susceptible to the phenomenon of adhesive breakage, hindering instrument-scale replication of cohesive breakage processes. Adhesive breakage measurements are notoriously irreproducible, due to strongly non-affine gel deformation. Efforts to ensure mechanical fixation give rise to spatially inhomogeneous deformation fields in the measuring geometry, particularly with respect to azimuthal and radial location. In order to elucidate the functional role of mechanically fixating geometries during gel breakage processes, 3 model solutions were prepared containing 5 wt%, 7.5 wt%, and 10 wt% macro-crystalline wax in dodecane. Rheograms were acquired in controlled deformation mode at imposed shear rates in the range of 0.1 - 1.0 s^{-1} using a vane or a cone and plate geometry. Yield stress values, nominally ascribed to primary peak height, were established based on 95% confidence intervals. Yielding trends confirm that adhesive breakage is particularly pronounced in high solid-fraction gels. A solid-fraction threshold delineates cohesive breakage in low solid-fraction gels from inherent adhesive breakage in high solid-fraction gels. Mechanical fixation in a vane geometry precludes wall slippage, ensuring cohesive breakage; resultant yield stress values follow a modified power-law dependency on total wax content, characterized by a power law exponent of $\sim$1.25. Nonuniform deformation within the vane geometry confers a modest (artificial) reduction in apparent yield stress value as a consequence of azimuthal integration of the torque signal. Nonuniform deformation also confers a distinct (artificial) broadening of the breakage peak, and is accompanied by the appearance of a new shoulder-peak located at a deformation value of $\sim$5. Conversely, in the cone and plate geometry, adhesive breakage occurs inherently for high solid-fraction gels, and is manifested by a substantial reduction in measured yield stress, albeit without a concomitant peak broadening. Hence, the practical utility of the cone and plate geometry is limited to low solid-fraction gels that inherently exhibit cohesive breakage behavior. Mechanical fixation afforded by the vane geometry effectively precludes wall slippage, enhancing measurement reproducibility while simultaneously ensuring cohesive breakage of high solid-fraction wax-gels that otherwise rupture in adhesive mode.

Introduction

Paraffin wax exists as indigenous components of many petroleum fluids, and comprises heavy linear, branched, and cyclic alkanes of the formula $C_nH_{2n+2-2c}$, where the symbol n denotes the number of carbon atoms and the symbol c denotes the number of cyclic rings in the molecular structure. The composition of wax is dominated by lower carbon-number n-alkanes

and higher carbon-number *iso*-alkanes and *cyclo*-alkanes.[1] Paraffin wax is often categorized as micro-crystalline or macro-crystalline, which may be isolated from distillate fractions above and below 460 ℃, respectively.[2] Macro-crystalline wax contains predominantly linear alkanes, with a smaller content of branched and cyclic alkanes. Micro-crystalline wax contains predominately branched and cyclic alkanes, with a smaller content of linear alkanes. The total wax content of petroleum fluid varies considerably, depending on geographic origin.

Petroleum fluids are often transported via pipeline through subsea environments. In geological reservoirs, petroleum fluid often exists at high temperature (70-150 ℃) and elevated pressure (greater than 2000 psi) conditions.[3] At the inlet of a subsea pipeline, paraffin wax is typically soluble in the petroleum fluid, which exhibits Newtonian flow properties, as illustrated in Figure 1(a). However, as heat is transferred to the seabed environment along the flow path, the fluid temperature often drops below the wax appearance temperature (WAT), and resultant wax precipitation gives rise to several flow assurance challenges. Wax deposits (not shown) may accumulate on internal pipe walls, driven by radial thermal gradients.[4] As low as 2% wax content in the fluid may cause wax deposition.[5] Wax deposits are known to harden via a counter-diffusion process termed aging,[6] in which the solid fraction increases with time. If a pipeline becomes completely constricted by deposits, flow ceases. Thermal, chemical or mechanical measures are often implemented on a periodic and remedial basis in order to sustain the flow process. For example, pigging may be periodically performed in order to mechanically remove solid wax deposits from internal pipe walls. If remedial measures are unable to control wax deposition, pipeline replacement or field abandonment may ensue.[7] Another flow assurance problem that arises due to wax precipitation is rheological gelling of the fluid, detailed in Figure 1(c). Upon periodic pipeline shut-in for planned maintenance or emergency contingencies, the fluid temperature will often drop below the gelation point. Consequently, gelling may occur rapidly within an entire pipe cross-section.[8] In the absence of radial thermal gradients, aging of wax-gels occurs by various mechanisms that do not involve a solid fraction increase, such as Ostwald ripening or Ostwald-related crystallization-fixation of crystal-crystal junctions, which is favorable on a free energy basis due to the sharp inverse curvature of crystal junction sites. Rheological gelling is typically addressed after the shut-in period by application of a substantial pressure-drop across the axial length of the pipeline. (Depressurization immediately after cooldown may serve to preemptively weaken the wax structure via gas expansion and counteract aging.) Upon restart, if the available pressure drop is insufficient to displace the gel, and heating methods are unavailable, the pipeline may need to be drilled through or alternatively replaced. Pour point depressants or yield point depressants are typically added to waxy petroleum fluids prior to shut-in, in order to mitigate gelling.[2,9] A final flow assurance problem that arises due to wax precipitation is stabilization of emulsions in the production train, which hinders separation processes. Economically, paraffin wax poses a billion dollar problem for the petroleum industry.[4]

When the temperature of a petroleum fluid drops below the WAT, the viscosity increases due to wax precipitation, and ultimately non-Newtonian flow behaviour results from crystal-crystal interactions in the bulk fluid.[8] The gel formation process comprises three stages; nucleation, growth, and agglomeration.[9–11] The rate at which these stages occur is dependent upon thermal history, temperature, shear rate, solvent quality, as well as the wax composition. Macro-crystalline paraffin wax crystallizes into platelet-like structures, as illustrated in Figure 1(b).[12] Below the gelation temperature, linear alkane components tend to form a volume-spanning network of plate-like crystals, entraining the liquid oil phase and forming a colloidal or physical gel, as illustrated in Figure 1(c). Affinity between wax crystals arises due to London van der Waals dispersion forces, conferring upon the wax structure a distinct mechanical strength.[13] A mechanical stress must be applied to rupture the gel and induce irrecoverable deformation and flow.[14] After the crystal net-

(a) At the pipe entrance, wax is soluble in the petroleum fluid, which exhibits Newtonian flow properties

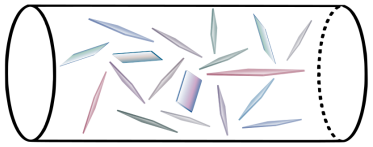

(b) After flow shut-in, the fluid cools below the WAT, and thin platelet-like wax crystals begin to appear in the fluid

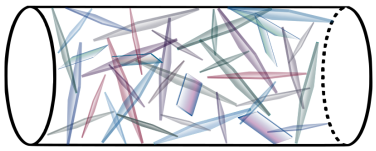

(c) The fluid cools below the gel point. A wax-oil gel plug forms, and subsequently hardens via a colloidal aging process

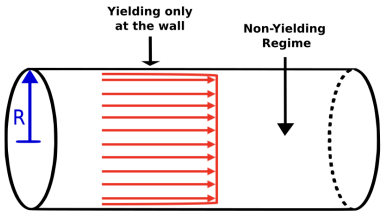

(d) Adhesive rupture (*i.e.* plug flow) of *strong* wax-oil gels upon pressure reapplication and flow restart

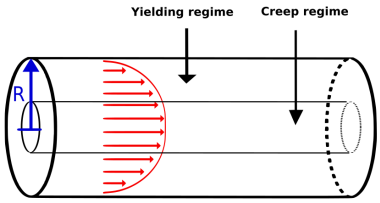

(e) Cohesive rupture (*i.e.* bulk shearing flow) of *weak* wax-oil gels upon pressure reapplication and flow restart

Figure 1: Wax-gel formation & breakage mechanisms

work begins to rupture due to the applied shear stress, the ability of the gel to resist deformation progressively diminishes. Hence, the yield stress reflects the gel strength. The breakdown mechanism can be either cohesive, resulting from the breakdown of the gel structure itself, or adhesive, caused by breakage at the pipe-gel interface.[15] Cohesive breakage occurs primarily in weak gels with a low wax content, while adhesive breakage is more pronounced in strong gels with a high wax content. These mechanisms are depicted in Figures 1(e) and 1(d), respectively. The gel network can, to some extent, behave as a visco-elastic material exhibiting creep; a time-dependent increase in strain when subjected to a constant stress. However, beyond the initial yielding event, wax-gels exhibit rheomalaxis behaviour, in which differential imposed deformation causes irreversible changes in the structural state. For semi-crystalline polymers the yield point can be understood as the boundary between elastic (*i.e.* recoverable) deformation and irreversible deformation. Analogously, the yield point for a wax-oil gel can be understood as the onset of breakage of the network, causing mechanical rupture of the gel network and enabling irrecoverable flow.[16] Quantitatively, the yield point of a wax-oil gel can be understood as the boundary between a primarily elastic response to differential imposed deformation and a primarily irreversible response to differential imposed deformation (*i.e.* rheomalaxis).

Various factors influence wax-gel rheology, including thermal history, baric history, deformation history, and fluid composition. The current investigation aims elucidate the role of mechanical fixation on the rheology of model wax-oil gels. Mechanical fixation is a technique that is relevant for rheometric measurement of recovered wax deposits as well as colloidal wax-gels formed upon homogenous cooling. Rheograms of model macro-crystalline wax-oil gels are acquired at various shear rates and wax compositions. Comparisons are made between a cone and plate geometry and a vane geometry with respect to reproducibility and the influence of shear rate and wax content. The vane method has been previously demonstrated to be advantageous in rheological studies of various materials, due to preclusion of wall slip during testing.[17] Cone and plate measuring geometries are widely used for wax-gels,[10,13,18] and a comparison between the two geometries reveals mechanistic knowledge pertaining to rheomalaxis.

Experimental

Solution preparation

Fluid samples were prepared by dissolving macro-crystalline Sasolwax 5405 in *n*-dodecane (ReagentPlus from Sigma-Aldrich). Dodecane has a molecular weight of 170.33 g/mol and a density of 0.75 g/cm^3 at 25 ℃. The mass fraction purity (CAS 112-40-3) is ≥0.99. Samples were prepared containing 5 wt%, 7.5 wt% and 10 wt% Sasolwax 5405, respectively. Previously performed gas chromatography analysis indicates that 77.6 wt% of the wax consists of linear paraffin components, while 22.4 wt% of the wax consists of branched and cyclic alkanes.[13]

For each model fluid sample, the thermal history was first erased. Experiments performed with samples influenced by thermal history are not representative of an initial homogeneous liquid phase, because dispersed crystallites are retained in the fluid and the nucleation, crystallization and agglomeration processes become influenced by the crystallite presence. As outlined by Paso et. al.,[13] the thermal history of a waxy petroleum fluid can be erased by heating the sample to a temperature of at least 20 ℃ higher than the WAT.[19] Therefore, prior to measurement, each prepared solution was thermally preconditioned by placing the solution in a heating oven maintained at a temperature of at least 60 ℃ for a time period of at least one hour in order to ensure that any prior thermal history would not influence the measurements, and that the initial sample state is a homogeneous liquid phase. The thermal preconditioning process ensures complete solubilization of any potential wax nucleates prior to initiating the thermal protocol, thereby ensuring an experimentally reproducible and homogeneous nucleation process, as well as optimal conditions for achieving adequate experimental reproducibility in the subsequent crystallization, agglomeration, and gel breakage processes.

Rheometric Protocol

A controlled-stress Anton Paar 14CR Physica MCR 301 rheometer equipped with Rheoplus software was used to prepare and analyze wax-oil gels derived from the model fluid solutions. The rheometer was first equipped with a CP40-2/S 2.009° cone and plate geometry of 3.9975 cm cone diameter and with a measuring gap size of 0.17 mm. The contact surface of the cone is sandblasted, and a sandblasted lower plate was used in conjunction with the sandblasted cone surface. The rheometer was also fitted with a 4-bladed ST22-4V-40 vane and CC27/T200 cup geometry. The active length of the 4-bladed vane is 111.5 mm. The measuring geometry types are illustrated in Figure 2. A Peltier element in thermal communication with both geometries provides thermal regulation to the model fluid in the rheometer.

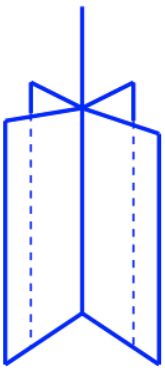

(a) 4-bladed vane geometry

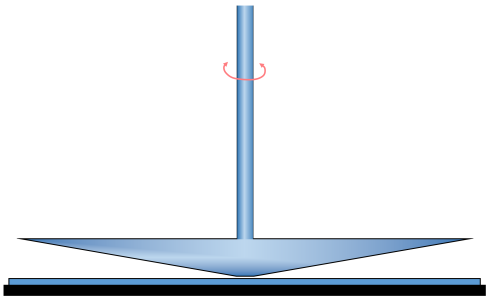

(b) Cone and plate geometry

Figure 2: Rheometric measuring geometries

For each experimental run, prior to loading the thermally preconditioned fluid sample into the respective geometry, the geometry was first cleaned with toluene and subsequently cleaned with acetone in order to facilitate drying.

For the vane geometry, the cleaned vane and cup were preheated at 60 ℃ in the oven for 30

minutes prior to loading the thermally preconditioned model fluid into the cup. Preheating of the vane and cup was performed in order to prevent the solution temperature from dropping below 60 ℃ during the loading process. Loading of the thermally preconditioned fluid sample into the thermally preconditioned cup occurred inside a fume hood. In order to ensure that the vane geometry was completely covered, a volume of approximately 40 mL of the model solution was loaded into the cup for each measurement. After loading of the thermally preconditioned fluid sample into the cup, the cup was installed on the rheometer, and then the preheated vane was installed on the rheometer and brought into the measuring position.

For the cone and plate geometry, the cleaned cone and plate was first installed on the rheometer and then brought to the measuring position. Subsequently, the cone and plate geometry was thermally regulated to a temperature of 60 ℃. Finally, the thermally preconditioned fluid sample was loaded into the cone and plate geometry. Because of the close proximity between the cone and the plate, fluid sample loading was not performed in a fume hood.

After loading of the thermally preconditioned fluid sample into the respective thermally preconditioned measurement geometry, a thermal protocol was applied to the sample under quiescent conditions. Samples were initially cooled from 60 ℃ to 42 ℃ at a rate of 5 ℃ per minute. The cooling rate was subsequently reduced to 1 ℃ per minute until the measurement temperature of 4 ℃ was reached. The sample was maintained quiescently at 4 ℃ for two minutes prior to application of the subsequent shearing protocol. The thermal protocol uses cooling rates that are marginally higher than a representative rate of cooling in a pipeline for the case of a shut-in operation, as the seabed temperature is typically ∼4 ℃, fluid entering the pipeline typically has a temperature within the range of 70 ℃ to 150 ℃,[10] and the pipeline wall provides a substantial thermal insulation effect.

A constant shear rate was imposed upon the gel during the shearing protocol. A short data sampling interval was utilized at low deformation values in order to properly measure incipient yielding dynamics, and a longer data sampling interval was utilized at larger deformation values in order to prevent data overload in the rheometric control system. Appropriate data sampling intervals were specified for each imposed shear rate condition.

Rheological measurements were conducted at 4 ℃ using constant imposed shearing rates of 0.1 s^{-1}, 0.5 s^{-1}, and 1.0 s^{-1}, respectively. After each experimental run, the used model fluid sample was discarded, and fresh thermally preconditioned fluid was used in subsequent runs.

Results and discussion

Rheomalaxis profiles in the cone & plate versus vane geometry

Measured rheomalaxis profiles are presented for the various wax-gel compositions obtained with both measurement geometries. Observed yielding trends are discussed in terms of gel strength, yield strain, breakage mechanism, rheomalaxis profile, and experimental reproducibility. Measured gel strength is quantified by the yield stress value, ascribed to nominal peak height. Mean yield stress values and associated 95% confidence intervals are listed in Table 1.

5 wt% composition

Three repeated experiments were performed for the 5 wt% solution of 5405 Sasolwax dissolved in dodecane using the vane geometry, and four repeated experiments were performed using the cone and plate geometry, at a prescribed shear rate of 0.1 s^{-1}.

At a shear rate of 0.1 s^{-1}, the vane geometry yields a lower peak shear stress value, 243.1 ± 6.44 Pa, in comparison to the cone and plate geometry which yields a peak shear stress value of 505.8 ± 29.9 Pa, as shown in Figures 3 and 4, respectively. The overall shape of the repeated rheograms obtained from each individual measuring geometry are remarkably reproducible up to large strain values (∼1000%), confirming a high degree of consistency in the associated nucleation, crystallization, agglomeration,

Table 1: Yield stress values with calculated 95% confidence intervals for the 5.0 wt%, 7.5 wt% and 10.0 wt% solutions given the selected geometries at shear rates of 0.1 s^{-1}, 0.5 s^{-1}, and 1.0 s^{-1}, respectively

Wax composition by weight [%]	**Vane geometry yield stress [Pa]**			**Cone & plate geometry yield stress [Pa]**		
	0.1 s^{-1}	0.5 s^{-1}	1.0 s^{-1}	0.1 s^{-1}	0.5 s^{-1}	1.0 s^{-1}
5.0	243.1 ± 6.44	629.8 ± 3.97	683.1 ± 11.0	505.8 ± 29.9	1,114 ± 211	–
7.5	4,498 ± 98.3	5,405 ± 281	6,397 ± 580	457.7 ± 41.1	754.7 ± 108	1,069 ± 110
10.0	9,440 ± 825	12,346 ± 936	13,355 ± 870	679.3 ± 10.6	921.1 ± 192	1,212 ± 244

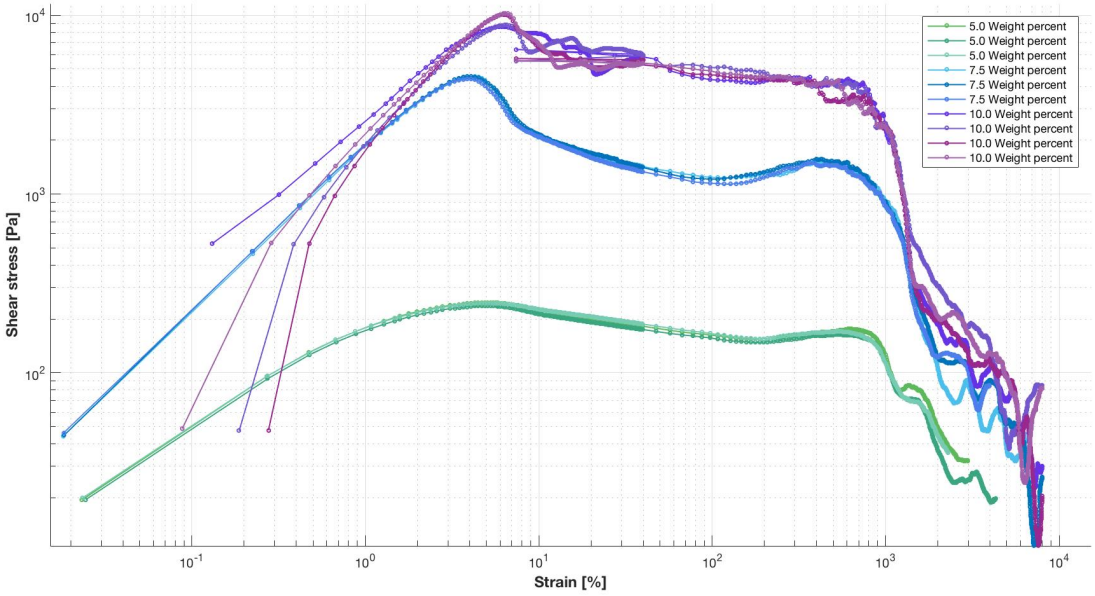

Figure 3: Vane geometry at a shear rate of 0.1 s^{-1}

and rheological gel breakage processes. The observed reproducibility in the rheogram profiles for the 5 wt% wax-gel demonstrates that methodical implementation of cleaning routines, thermal preconditioning routines, and thermal protocols is highly effective in establishing repeatability of rheometric gel breakage measurements. Consistency in cleaning routines is particularly important for achieving reproducible gel breakage measurements, due to the influence of the cleaning protocol on surface wettability conditions, adsorbed moisture films, and resultant gel adherence.

The reduced peak yield stress value measured in the vane geometry, as compared to the cone and plate geometry, is attributable to nonuniform deformation and nonuniform yielding in the vane geometry, particularly with respect to azimuthal position. (In contrast, in cohesive breakage mode, the cone and plate geometry facilitates affine shear deformation and a spatially-uniform yielding event.) In the vane geometry, when the blades exert shear stress onto the gelled fluid, the resultant shear deformation field exhibits large gradients in the radial and azimuthal directions, particularly in the vicinity of the blade edges. These shear deformation gradients are particularly pronounced within the radial deformation band located between the blade edges and the inner wall of the cup. As a consequence of azimuthal integration of the torque signal, stress signals originating from localized azimuthal yielding positions become averaged together with stress signals originating from non-yielding azimuthal positions. Hence, azimuthal integration of the

torque signal effects a distinctive broadening of the measured breakage peak and a concomitant reduction in peak height. A new shoulder peak also appears at an absolute shear deformation value of ∼5. Overall, the results confirm that for the low wax content of 5 wt%, the cone and plate measuring geometry provides a more accurate representation of the true cohesive yield stress value in comparison to the vane measuring geometry. For the low wax content of 5 wt%, gel breakage occurs cohesively in the cone and plate geometry at a shear rate of 0.1 s^{-1}, as confirmed by the higher peak shear stress obtained in the cone and plate as compared to the vane geometry (which ensures cohesive rupture) at the same nominal shear rate condition. Therefore, in the cone and plate geometry, the shear deformation field is largely uniform with respect to radial, angular, and azimuthal position. Hence, the combined conditions of (1) confirmed cohesive breakage (due to the low wax content) and (2) a uniform shear deformation field, result in the cone and plate measuring geometry establishing a more accurate representation of the true cohesive yield strength of the wax-gel than the vane measuring geometry, at a shear rate of 0.1 s^{-1}.

In the cone and plate geometry, the maximum shear stress occurs at a shear deformation value of 0.6% at a shear rate of 0.1 s^{-1}. Hence, the yield strain value is 0.6% for the cone and plate geometry at a shear rate of 0.1 s^{-1}. Because of the combined conditions of (1) the uniform shear deformation field in the cone and plate geometry and (2) an absence of adhesive breakage at the low shear rate of 0.1 s^{-1}, the yield strain value of 0.6% is considered to represent the inherent yield strain property of the 5 wt% wax-oil gel at an imposed shear rate of 0.1 s^{-1}.

At a shear rate of 0.1 s^{-1}, the nonuniform shear deformation field in the vane geometry confers an artificial increase in apparent yield strain value to 5%, representing nearly an entire order-of-magnitude increase in the apparent yield strain value, attributed to nonuniform deformation in the vane geometry. The artificial increase in yield strain for the vane geometry facilitates optimal spacing of data points near the peak, because the rheometer has additional time to obtain data points prior to the yielding event and near the peak when the yielding event is artificially shifted to a higher strain value. In addition, the nonuniform shear deformation field in the vane geometry results in a broader, smoother breakage peak on the rheogram, such that the peak height may be easily characterized while retaining a relatively large spacing interval between data points.

Three parallels were run with the vane geometry and two parallels were run with the cone and plate geometry at a prescribed shear rate of 0.5 s^{-1}. Yield stress values were found to be 629.8 ± 3.97 Pa and $1,114 \pm 211$ Pa for the vane geometry and cone and plate geometry, respectively. Rheograms obtained using the vane geometry at a shear rate of 0.5 s^{-1} are shown in Figure 6. The vane geometry displays excellent reproducibility as well as adequate spacing of data points in the vicinity of the peak of the curve, due to the artificial increase in apparent yield strain value caused by nonuniform gel deformation. In contrast, at the increased shear rate of 0.5 s^{-1} with the cone and plate geometry, the rheometer has insufficient time to obtain sufficient data points prior to the yielding event that inherently occurs in the vicinity of 0.6% strain. In addition, the rheometric control system has insufficient time to stabilize the prescribed shear rate prior to the yielding event at the faster imposed shear rate of 0.5 s^{-1}. Hence, a transient instability in shear rate coincides with the yielding event, resulting in a truncated stress peak, as shown in Figure 5. Nevertheless, a higher peak maximum is observed for the cone and plate geometry at a shear rate of 0.5 s^{-1} in comparison to a shear rate value of 0.1 s^{-1}.

At an imposed shear rate of 1 s^{-1}, three parallels were conducted with the vane geometry and several parallels were conducted with the cone and plate geometry. Rheograms obtained using the vane geometry are shown in Figure 9.

For the cone and plate geometry at a shear rate of 1 s^{-1}, due to the fast shear rate, low gel solid fraction, and limited data sampling frequency, the measurement is unable to properly probe the yielding peak. No data points were obtained in the vicinity of the peak, and the first meaningful data point appears at strain

value of approximately 3%, in comparison to the inherent yield strain value of the gel in the vicinity of 0.6%. As such, the nominally measured yielding behavior of the gel at a shear rate of 1 s^{-1} is not representative of the material property of the gel. Due to the absence of data points over an extended deformation range in the vicinity of the yielding peak, the yielding behavior of the weak 5 wt% gel at a shear rate of 1 s^{-1} is unable to be probed using the cone and plate geometry, and is therefore not included in Table 1.

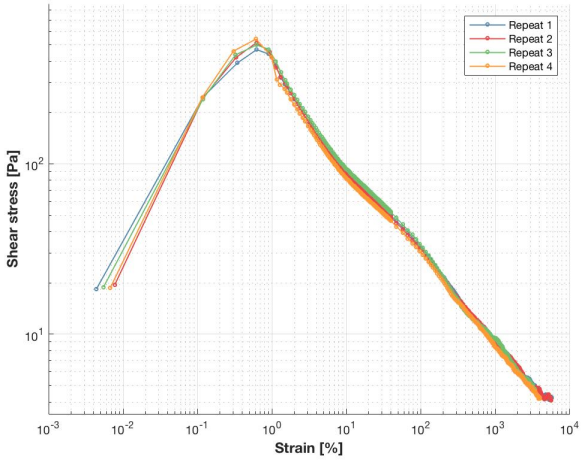

Figure 4: Cone and plate geometry. 5 wt% solution at a shear rate of 0.1 s^{-1}

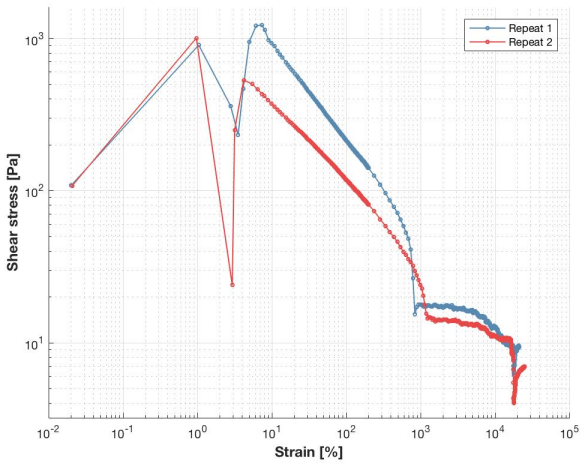

Figure 5: Cone and plate geometry. 5 wt% solution at a shear rate of 0.5 s^{-1}

In the vane geometry, the large apparent yield strain value is attributed to nonuniform shear deformation and the azimuthal averaging effect, and the mean yield stress value is 683.1 ± 11.0 Pa. Hence, at the fast shear rate of 1 s^{-1}, only results from the vane geometry are considered to be valid. The ability of the vane measuring geometry to accurately probe the yielding process at a shear rate of 1 s^{-1} is attributed to the artificial shift in the apparent yielding strain to higher deformation values. However, even with the additional benefit of the artificial increase in the apparent yield strain, a distinct scarcity of data points is still observed in the vicinity of the breakage peak in Figure 9 for the 5 wt% wax-oil gel, due to the fast shear rate of 1 s^{-1} in conjunction with the limited data sampling frequency of the instrument.

7.5 wt% composition

During a rheometric experiment, a phenomenon known as slippage may occur, especially in high solid fraction dispersions such as wax-oil gels. According to Barnes,[20] wall slip is due to displacement of the disperse phase away from solid boundaries in a two-phase system. High molecular weight molecules are more vulnerable to slip than other molecules, and high solid fraction dispersions are typically more vulnerable to slippage than low solid fraction dispersions. The cone and plate geometry is more susceptible to slippage due to an absence of large-scale fixating features, whereas the blades of the vane provide mechanical fixation and preclude slippage. In the vane geometry, the shearing band occurs away from the blades. According to Rønningsen,[18] the solution yields within itself when the vane is used, eliminating slippage.

If slippage occurs only after a yielding event, then the yield strain would hypothetically remain unaffected. However, because slippage often occurs near the stress maximum, the slippage phenomenon usually coincides with the yielding event. Because of the concurrent slippage and adhesive breakage (*i.e.* rupture) processes unique to high solid-fraction wax-oil gels formed on solid surfaces, the slippage terminology is generally used synonymously with the adhesive breakage terminology for wax-oil gels initially adherent to solid surfaces.

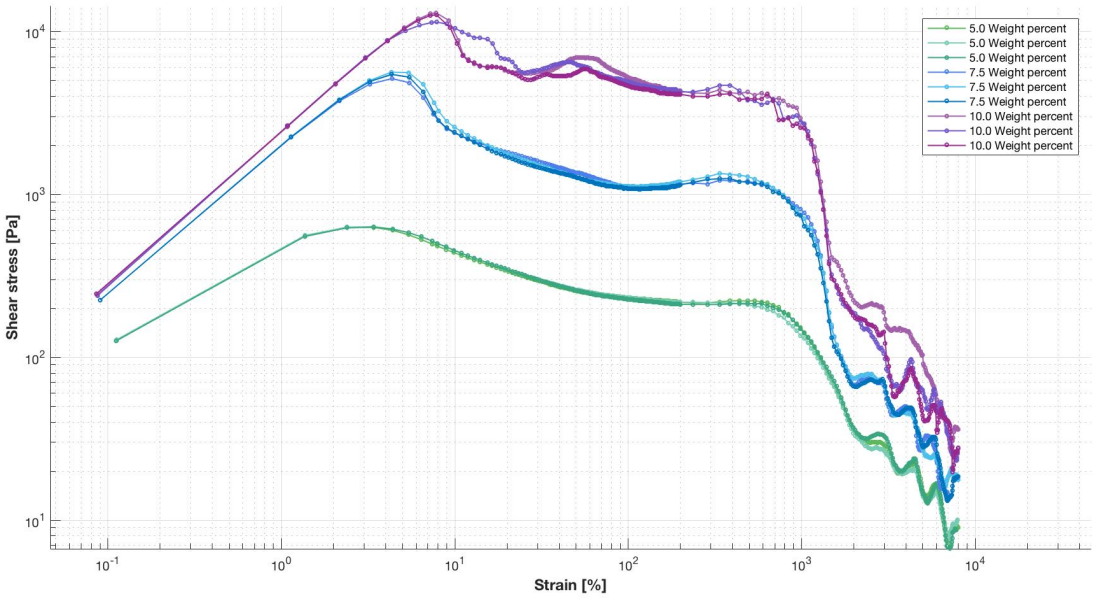

Figure 6: Vane geometry at a shear rate of 0.5 s^{-1}

Three repeated measurements were conducted for the 7.5 wt% solution at a shear rate of 0.1 s^{-1} for the cone and plate geometry and three measurements were conducted for the vane geometry. Obtained rheograms are shown in Figure 7 and Figure 3, respectively.

For the cone and plate geometry, the nominally measured shear stress peak for the 7.5 wt% solution occurs at a shear strain value of 2%, which is higher than the 0.6% yield strain value for the 5 wt% solution. The increase in yield strain with increasing wax content is likely attributable to a combination of 2 distinct effects: (1) a higher inherent yield strain for the higher solid-fraction gel. Increased solid fractions likely lead to additional mechanisms for crystal rearrangement prior to yielding due to the more abundant crystal-crystal contacts, in comparison to lower solid fraction gels that exhibit more sparse contacts points between individual wax crystals, and (2) an artificially induced increase in the observed yield strain as a result of the adhesive breakage mechanism, meaning that substantial gel slippage may occur on the measurement surface prior to the maximum stress signal being recorded (corresponding to the maximum tolerated straining of the wax network). The two combined effects most likely account for the increase in measured yield strain for the 7.5 wt% solution of 2% in comparison to the inherent representative yield strain of 0.6% for the 5 wt% solution.

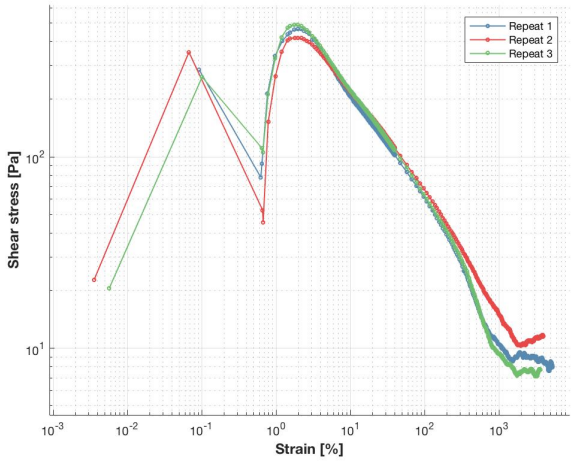

Figure 7: Cone and plate geometry. 7.5 wt% solution at a shear rate of 0.1 s^{-1}

The apparent measured yield strain value for the 7.5 wt% solution is artificially increased to ∼4% in the vane measuring geometry, in comparison to the measured yield strain of ∼2% for the 7.5 wt% solution in the cone and plate geometry, due to nonuniform gel deformation in the vane measuring geometry. The nominally

measured yield strain value of 4% is therefore not representative of the material property of the gel. However, as a consequence of the artificial increase in apparent yield strain value, the rheometric control system has sufficient time to acquire sufficient data points in the vicinity of the yielding peak, providing confidence in the resultant measured cohesive yield stress values.

At a shear rate of 0.1 s^{-1}, the peak shear stress values were found to be 457.7 ± 41.1 Pa for the cone and plate geometry and $4,498 \pm 98.3$ Pa for the vane geometry. The strong increase in cohesive yield stress of the 7.5 wt% solution in comparison to the 5 wt% solution, as measured using the vane geometry, is attributable to the power law dependency of the gel strength with respect to total wax content. The increased strength of the 7.5 wt % gel in comparison to the 5 wt % gel is not reflected in the cone and plate geometry, because the strong gel undergoes breakage in the adhesive mode in the non-fixated geometry, even when utilizing roughened sandblasted contact surfaces of the cone and the plate.

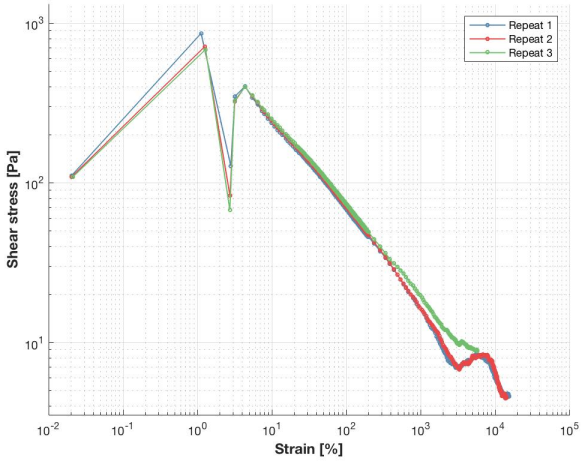

Figure 8: Cone and plate geometry. 7.5 wt% solution at a shear rate of 0.5 s^{-1}

At a shear rate of 0.5 s^{-1}, three measurements were performed with both measuring geometries. Rheograms obtained with the vane geometry are shown in Figure 6, and confirm excellent experimental reproducibility and a high cohesive gel strength for the 7.5 wt% solution.

Figure 8 shows rheograms obtained with the cone and plate measuring geometry at an imposed shear rate of 0.5 s^{-1}. Two distinct peaks are observed in the stress profile, and are attributed to an instability in the shear rate coinciding with the peak maximum at the prescribed shear rate of 0.5 s^{-1}. 95% confidence interval yield stress values for the cone and plate geometry listed in Table 1 are based upon the maximum peak shear stress values, irrespective of where the peak maximum appears on the rheogram. Because of the distinct phenomenon of adhesive breakage occuring at 0.5 s^{-1}, the yield stress values obtained from the cone and plate geometry, 754.7 ± 108 Pa, are less representative of the inherent gel strength than the cohesive yield stress values obtained from the vane geometry, $5,405 \pm 281$ Pa.

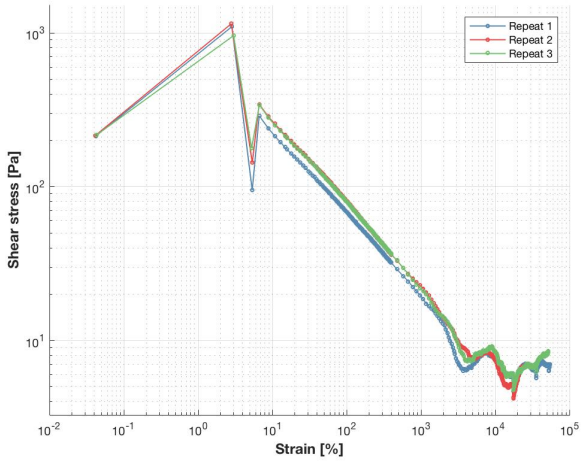

Figure 10: Cone and plate geometry. 7.5 wt% solution at a shear rate of 1 s^{-1}

At a shear rate of 1 s^{-1}, two repeated measurements were conducted with the vane geometry and three repeated measurements were conducted with the cone and plate geometry for the 7.5 wt% solution. The acquired rheograms are shown in Figures 9 and 10, respectively. Peak shear stress values were found to be $6,397 \pm 580$ Pa for the vane geometry, and $1,069 \pm 110$ Pa for the cone and plate geometry, consistent with a substantial reduction in the apparent yield stress value associated with the adhesive breakage mechanism.

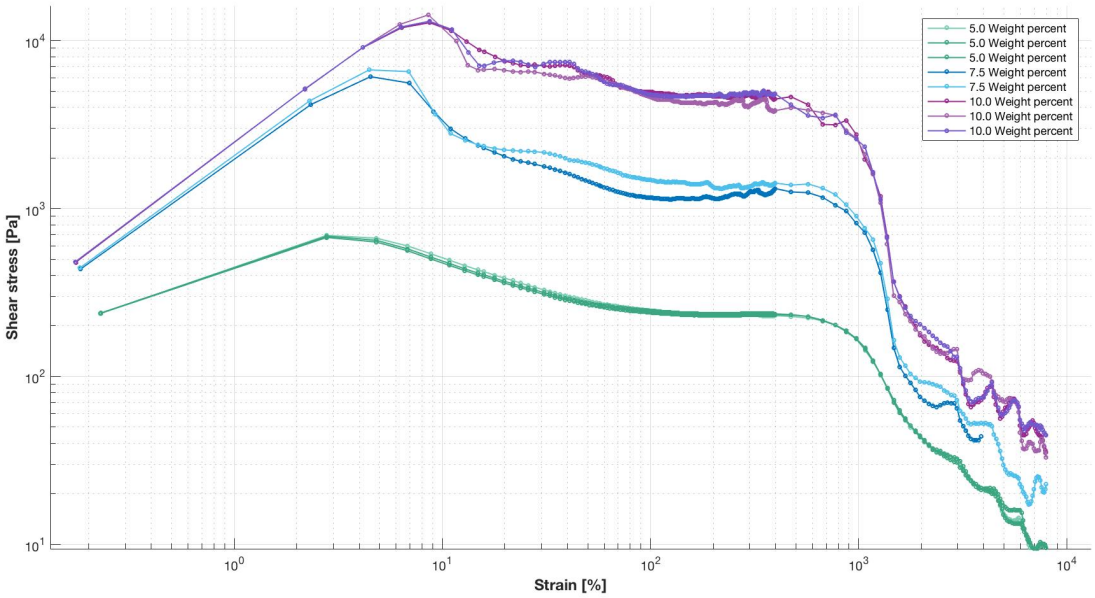

Figure 9: Vane geometry at a shear rate of 1 $s^{-}1$

10 wt% composition

A very high cohesive gel strength is measured with the vane geometry for the 10 wt% solution at a prescribed shear rate of 0.1 s^{-1}, as evident in Figure 3. Analogous rheograms obtained using the cone and plate geometry are shown in Figure 11. Yield strain values obtained using the vane geometry are in the vicinity of 6.5%, and yield strain values obtained using the cone and plate geometry are in the vicinity of 4%. Table 1 indicates that the cone and plate geometry establishes an adhesive yield stress of 679.3 ± 10.6 Pa. The adhesive yield stress value is less representative of the inherent gel strength than the cohesive yield stress value of $9,440 \pm 825$ Pa obtained from the vane geometry.

At a shear rate of 0.5 s^{-1}, rheograms acquired from the cone and plate geometry display a distinct split peak, as shown in Figure 12. Calculated confidence intervals are determined based on maximum nominal shear stress values for each respective rheogram. Based on established 95 % confidence intervals shown in Table 1, it is evident that the vane geometry, with a shear stress peak value of $12,346 \pm 936$ Pa, provides a more accurate representation of the gel strength than the cone and plate geometry, with a peak maximum of 921.1 ± 192 Pa.

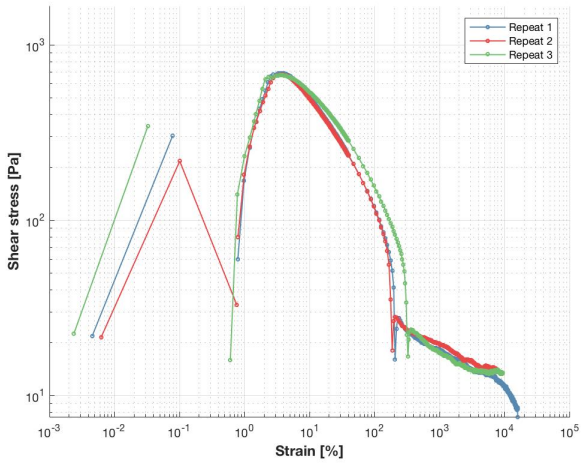

Figure 11: Cone and plate geometry. 10 wt% solution at a shear rate of 0.1 s^{-1}

At a shear rate of 1 s^{-1}, three repeated measurements were conducted with the vane geometry. Figure 9 shows the obtained rheograms, illustrating adequate reproducibility. The cohesive yield stress measured with the vane geometry is $13,355 \pm 870$ Pa. Five repeated measurements were conducted with the cone and plate geometry. The rheograms, shown in Figure 13, display adequate reproducibility. Apparent yield strain values are in the vicinity of

2-3%. The yield stress confidence interval for the cone and plate geometry is $1,212 \pm 244$ Pa.

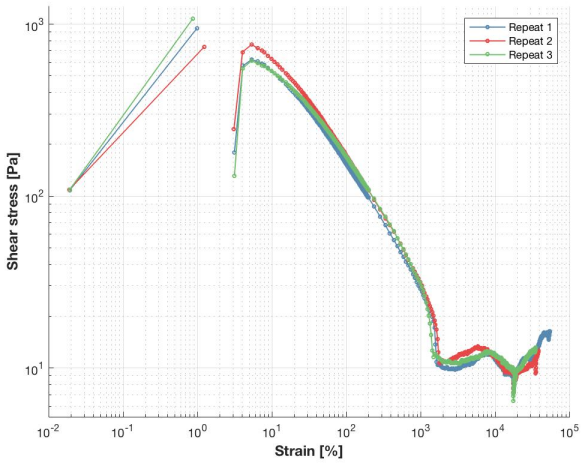

Figure 12: Cone and plate geometry. 10 wt% solution at a shear rate of 0.5 s^{-1}

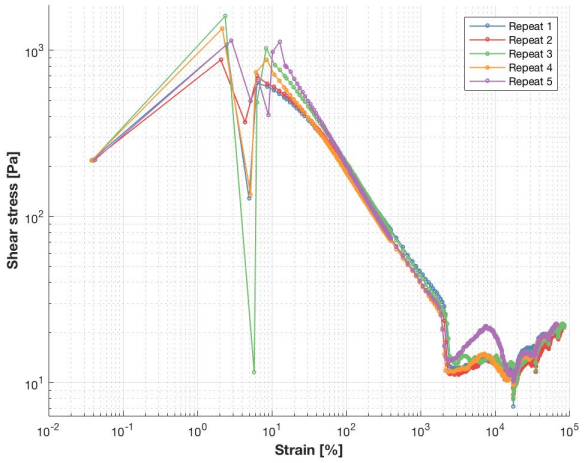

Figure 13: Cone and plate geometry. 10 wt% solution at a shear rate of 1 s^{-1}

Yield Stress Trends

Apparent yield stress values for 5 wt%, 7.5 wt%, and 10 wt% compositions of Sasolwax 5405 dissolved in dodecane are plotted versus total wax content in Figure 14 for both the vane geometry and the cone and plate geometry. Vertical error bars shown in Figure 14 denote 95% confidence intervals, as listed in Table 1.

At each imposed shear rate condition, the apparent yield stress measured in the vane geometry increases with increasing wax content. In addition, the apparent yield stress measured in the vane geometry increases with increasing shear rate. Cohesive yield stress values obtained using the vane geometry are modelled as a modified power law function of the total wax content. The classic Bingham relation (utilizing a constrained ratio between the Bingham viscosity and the Bingham yield stress) is coupled to a modified power-law equation that directly informs the shear-rate invariant yield stress term τ_y, and also indirectly informs the Bingham viscosity term. The entire equation set used to model apparent yield stress values obtained from the vane geometry is:

$$\tau_{y,a} = \tau_y + \dot{\gamma}\mu_a \tag{1}$$

as informed by

$$\tau_y = A(\omega - B)^n \tag{2}$$

$$\mu_a/\tau_y = constant \tag{3}$$

In Equations 1-3, $\tau_{y,a}$ is the apparent yield stress, ω indicates the total wax content of the gel and n denotes the modified power-law exponent. The symbols A and B are heuristic fitting parameters. A standard least squares minimization routine is used to perform a unified fit of Equations 1-3 to the entire set of vane geometry yield stress values listed in Table 1. The resultant unified rheological parameters are shown in Table 2. The trend of the fitted mathematical model, as described by Equations 1-3 and informed by the parameter set listed in Table 2, is plotted in Figure 14 for each shear rate condition as dotted curves alongside the respective data point markers indicating the vane geometry yield stress values.

For the unified cohesive yielding trends, the modified power-law exponent is 1.25, and the ratio of Bingham viscosity to Bingham yield stress is 0.43. For cohesive measurements obtained with the vane geometry, the yield stress shows a weak monotonic increase with increasing shear rate at all wax compositions, lending credence to the obtained yield stress values. The weak dependence of cohesive yield stress with shear rate indicates that the measured co-

Table 2: Unified Rheological Parameters for Cohesive Yield Stress

Parameter	Unified Cohesive Prediction
B	4.53
n	1.25
A	1,117.8
μ_a/τ_y	0.43

hesive yield stress values provide a meaningful representation of the material property, and are not merely instrumental artifacts. Overall, the increase in cohesive yield stress with increasing shear rate is in accordance with the results obtained by Paso et. al.,[13] for which a cone and plate geometry was used for a sample that exhibits inherently cohesive yielding behavior. Hence, the collective data shown in Figure 14 reflect primarily an ideal yielding mechanical response that is independent of the shear rate, and reflects only a modest ideal shear-rate-dependent viscous contribution to the overall incipient cohesive rupture process.

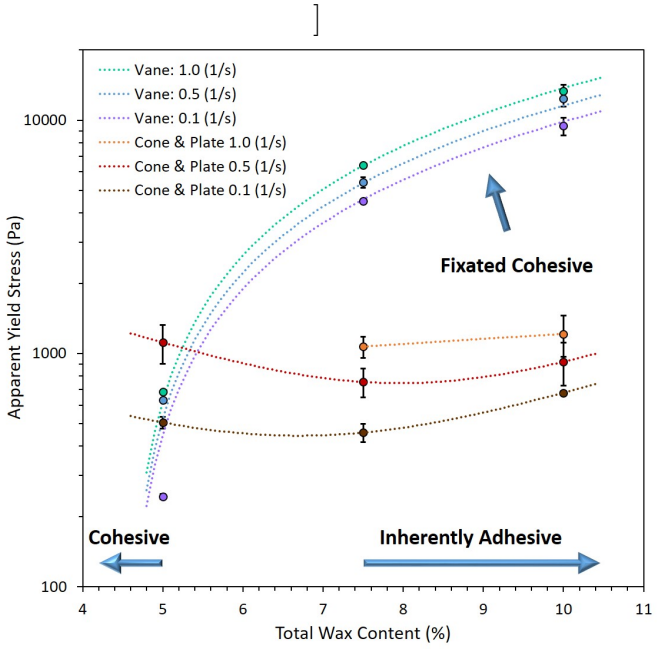

Figure 14: Measured yield stress values as a function of total wax content at the shear rate conditions of 0.1 s^{-1}, 0.5 s^{-1}, and 1.0 s^{-1}.

The apparent yield stress values measured in the cone and plate geometry are modeled separately for each imposed shear rate condition (*i.e.* 0.1 s^{-1}, 0.5 s^{-1}, and 1 s^{-1}), using a simple quadratic or alternatively linear fit. The fitted simple mathematical relations are plotted in Figure 14 as dotted curves alongside the data point point markers indicating the cone and plate geometry yield stress values.

Comparison of cohesive and adhesive breakage regimes universally shows a solid-content threshold delineating inherent cohesive breakage at 5 wt% wax from inherent adhesive breakage at 7.5 wt% and 10 wt% wax. Hence, a threshold between the 2 breakage regimes exists between 5 wt% wax and 7.5 wt% wax. The yielding trends obtained are qualitatively similar to the obtained values from Zhao et. al.[19] The error bars corresponding to the 5 wt% solution in the vane geometry are very small and are consistent with largely overlapping repeated rheograms for the 5 wt% solution shown in Figure 3, Figure 6, and Figure 9. The results demonstrate the potential for achieving excellent experimental reproducibility in yield stress measurements using the vane geometry, especially for low wax contents (*i.e.* 5 wt%). However, in the vane measuring geometry, the reproducibility of the rheogram profiles decreases as the total wax content increases, as evidenced by the 95% confidence intervals listed in Table 1 as well as the relative size of the error bars shown in Figure 14.

For the cone and plate geometry, at imposed shear rate conditions of 0.1 s^{-1} and 0.5 s^{-1}, the apparent gel strength decreases slightly from 5 wt% wax to 7.5 wt% wax prior to a modest increase in gel strength at a composition of 10 wt% wax. The reason for the reduction in apparent yield stress from 5 wt% wax to 7.5 wt% wax is attributed to the shift in breakage mechanism from cohesive to adhesive. The margin of error is in general quite high for adhesive breakage, due to the stoichastic processes as-

sociated with non-affine deformation and adhesive breakage. Hence, the observed reduction in apparent yield stress, corresponding to the shift in breakage mechanism accompanying the increased solid fraction, cannot be considered to be statistically significant.

For rheograms obtained with the cone and plate geometry, the yield stress values show a substantially stronger monotonic increase with increasing shear rate, signifying that the adhesive breakage mechanism is more sensitive to shear rate than is the cohesive breakage mechanism. Hence, in comparison to the vane geometry yield stress values, the adhesive breakage yield stress values reflect a larger ideal shear-rate dependent viscous contribution to the overall incipient mechanical response, and only to a lesser extent reflect a shear-rate invariant ideal yielding contribution to the overall incipient mechanical response. Figure 15 shows adhesive yield stress values obtained from the cone and plate geometry. Adhesive yield stress trends rigorously follow the Bingham relation, characterized by a shear-rate-invariant yield stress term of 399 Pa and 621 Pa for 7.5 wt% and 10.0 wt% solutions, respectively. The ideal viscous contribution term to the adhesive yield stress correlation is 677 Pa*s and 593 Pa*s for 7.5 wt% and 10.0 wt% solutions, respectively.

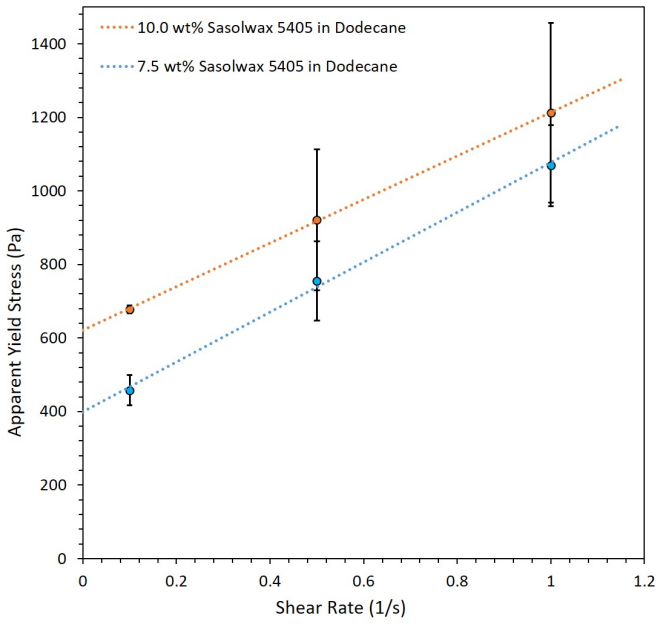

Figure 15: Yield stress versus shear rate for adhesive breakage measured with the cone and plate geometry

Conclusion

The geometry of the measuring device influences the nature of the shear deformation field imposed on the wax-oil gel sample during rheometric measurement. In the conventional cone and plate measuring geometry, affine (homogenous) deformation results from purely cohesive gel breakage observed at low wax contents. Non-affine deformation results from adhesive breakage of the model macro-crystalline wax-oil gel in the cone and plate geometry at high wax contents, despite utilization of sandblasted surfaces on both the cone and the plate. A transition is shown to occur from cohesive breakage to adhesive breakage behavior as the total macro-crystalline wax content in dodecane increases from 5 wt% to 7.5 wt%, indicating that an inherent solid-fraction threshold also exists for the transition. However, because macro-crystalline paraffin wax is partially soluble in dodecane at 4 ℃, the associated solid-fraction threshold likely exists somewhat below a value of 5 vol%.

In the vane geometry, on the other hand, adhesive breakage is invariably precluded for the model macro-crystalline wax-gel as a result of mechanical fixation, such that gel breakage occurs primarily in cohesive mode at all wax contents within the range 5 wt% to 10 wt% wax. However, localization of deformation in the near vicinity of the edges of the blades results in non-affine deformation fields in the vane geometry. The nonuniform shear deformation fields lead to an artificial increase in the apparent yield strain, an artificial reduction in peak height, a broadening of the associated breakage peak on the acquired rheogram, and the appearance of a new shoulder peak at an absolute shear deformation value of $\sim$5. With the vane geometry, the cohesive yield stress for the macro-crystalline wax-oil gel is shown to adhere to a modified power-law model with respect to total wax content, characterized by a modified power-law exponent of $\sim$1.25.

Cohesive yield stress values show little variation with imposed shear rate for the model wax-gel, indicating that the incipient yielding event is highly ideal, with only minimal viscous con-

tribution to the initial yielding response. The highly ideal nature of cohesive yielding confirms that structural yielding in the model wax-gel originates primarily from the irreversible rupture of crystallographic bonds between wax crystals, with only small viscous contributions associated with structural re-arrangement or solvent displacement processes. Adhesive yield stress values measured for the model wax-gel carry a much stronger viscous component, consistent with strong shear localization towards the vicinity of the yielding surface during incipient interfacial rupture associated with the adhesive breakage event.

In terms of analytical method development for waxy petroleum fluids, it may be concluded that the shear rate cannot become too fast for the cone and plate geometry in order to guarantee reproducibility, due to instrument-limited data point sampling intervals. Another disadvantage with the cone and plate is the vulnerability towards vibrations and instrumental instabilities. Based on 95% confidence intervals, the vane generally produces more reproducible yield stress values, because the yield strain is shifted towards higher values as a result of nonuniform deformation fields. Additionally, the risk of adhesive breakage is eliminated.

The gel strength of the model wax-gel increases as the wax content increases, with the exception of the transition from cohesive to adhesive breakage, as measured with the cone and plate geometry. Higher yielding stress values are observed for all model solution compositions as the shear rates increase, in accordance with classical mechanical stability considerations.

Based on the findings related to the experimental reproducibility of the 2 geometries, the effect of total wax content, and the influence of the shear rate, it is put forward by the operator to use the vane geometry as guideline for further studies in cases in which adhesive breakage may occur. However, the cone and plate geometry is superior for meaningful determination of the inherent yield strain and inherent yield stress values for cases of inherent cohesive breakage. Finally, new fixating geometries with reduced dimensions between fixating features may serve to minimize disparities between cohesive breakage observed in the cone and plate geometry and fixating geometries, affording more accurate measurements of cohesive breakage of high solid-fraction wax-oil gels that inherently break via the adhesive mode.

An important industrial implication of this work is that the effectiveness of surface roughness techniques depends largely on the lengthscale of the fixating features. The larger the lengthscale of the fixating feature, the more effective is the fixation in preventing slippage. Hence, serrated surfaces and grooved surfaces likely provide substantially improved fixating performance in comparison to sandblasted surfaces, due to the larger length-scale of the mechanical fixating features. As such, an important implication for analysis of recovered wax deposits of high solid content is that large-scale fixating features are necessary in order to successfully prevent slippage.

Operational knowledge pertaining to the wax-gel breakage mechanism and rheomalaxis profiles are paramount for large-scale prediction of pipeline restart behavior. Hence, realistic assessment of pipeline restartability depends on knowledge of gel breakage on both representative surfaces (*i.e.*, the inner pipeline wall) as well as on fixating surfaces in order to understand the cohesive yielding behavior. A complete understanding of rheomalaxis in both adhesive and cohesive mode, in conjunction with properly informed hydrodynamic computations, may ultimately provide qualified predictions of pipeline restart behavior in the field.

Associated Content

Supporting Information

Statistical theory as well as an equation set for calculating the 95% confidence intervals listed in Table 1, based on the assumption of a normal error distribution. This material is available free of charge via the Internet at http://pubs.acs.org.

References

(1) Kurniawan, M.; Subramanian, S.; Norrman, J.; Paso, K. *Energy&fuels* **2018**, *32*, 5857–5867.

(2) Paso, K. G. *Paraffin gelation kinetics*; University of Michigan, 2005.

(3) Huang, Z.; Lee, H. S.; Senra, M.; Fogler, H. S. *AlChE Journal* **2011**, *57*, 2955–2964.

(4) Singh, P.; Venkatesan, R.; Fogler, H. S.; Nagarajan, N. *AlChE Journal* **2000**, *46*, 1059–1074.

(5) Lashkarbolooki, M.; Seyfaee, A.; Esmaeilzadeh, F.; Mowla, D. *Energy&fuels* **2010**, *24*, 1234–1241.

(6) Paso, K.; Fogler, H. S. *Energy&fuels* **2004**, *18*, 10051013.

(7) Chen, X.; Butler, T.; Volk, M.; Brill, J. *Society of Petroleum Engineers* **1997**, 249–256.

(8) Zheng, S.; Saidoun, M.; Palermo, T.; Mateen, K.; Fogler, H. S. *Energy&fuels* **2017**, *31*, 5011–5023.

(9) Yang, F.; Zhao, Y.; Sjöblom, J.; Li, C.; Paso, K. G. *Journal of Dispersion Science and Technology* **2015**, *36*, 213–225.

(10) Singh, P.; Fogler, H. S.; Nagarajan, N. *Journal of Rheology* **1999**, *43*, 1434–1459.

(11) de Castro Machado, A. L.; Lucas, E. F. *Petroleum Science And Technology* **2007**, *17*, 1028–1041.

(12) Ferris, S. W.; Cowles, H. C. *Industrial & Engineering chemistry* **1945**, *37*, 1054–1062.

(13) Paso, K.; Kompalla, T.; Oschmann, H. J.; Sjöblom, J. *Journal of Dispersion Science and Technology* **2009**, *30*, 472–480.

(14) Hiemenz, P. C.; Rajagopalan, R. *Principles of Colloid and Surface Chemistry.*; CRC Press, Boca Raton, 3rd edition, 1997; p 464.

(15) Lee, H. S.; Singh, P.; Thomason, W. H.; Fogler, H. S. *Energy&fuels* **2008**, *22*, 480–487.

(16) Zhao, Y.; Paso, K.; Kumar, L.; Safieva, J.; Sariman, M. Z. B.; Sjöblom, J. *Energy&fuels* **2013**, *27*, 2025–2032.

(17) Li, M.; Sun, M.; Lu, Y.; Zhang, J. *Energy&fuels* **2017**, *31*, 11977–11986.

(18) Rønningsen, H. P. *Journal of Petroleum Science and Engineering* **1992**, *7*, 177–213.

(19) Zhao, Y.; Kumar, L.; Paso, K.; Ali, H.; Safieva, J.; Sjöblom, J. *Industrial Engineering Chemistry Research* **2012**, *51*.

(20) Barnes, H. A. *Journal of Non-Newtonian Fluid Mechanics* **1995**, *56*, 221–251.

Supporting Information

Confidence interval representation of wax-oil gel strength

Yield stress values, nominally ascribed to maximum peak height, are expected to be normally distributed, despite the high degree of variability in the stochastic stress signals associated with adhesive breakage processes. The sample standard deviation, Equation 5, was used to establish an estimate of the degree of variation in the measured yield stress values of the various model fluid compositions.

Experimental data points are located far from the mean value if the standard deviation value is large and are located closer to the mean value if the standard deviation value is small. When the margin of error is small, the reproducibility of the measurement is higher. Because deviations from the mean of the measured samples are by definition smaller than deviations

from the population mean, Equation 4 is utilized. Using 95 % confidence intervals provides a 95 % confidence that the unknown population mean will be captured within the obtained interval. Estimations were performed using the following mathematical formulas:

$$\overline{x} = \frac{1}{n}\sum_{i=1}^{n} x_i, \tag{4}$$

$$s = \sqrt{\frac{1}{n-1}\sum_{i=1}^{n}(x_i - \overline{x})^2} \tag{5}$$

In Equations 4 and 5, n is the number of samples, x_i indicates the yield stress of the sample, $\overline{x}$ represents the mean of all the samples and s is the sample standard deviation.

In other words, the gel strength is represented as a range of values, where the estimate is the mean of the samples:

$$estimate = \pm\ margin\ of\ error \tag{6}$$

The margin of error for a 95 % confidence interval is calculated from:

$$m = 1.96\frac{s}{\sqrt{n}} \tag{7}$$